Temperature-Dependent Electrical Transport in Polymer-Sorted Semiconducting Carbon Nanotube Networks

*Jia Gao and Yueh-Lin (Lynn) Loo**

The temperature dependence of the electrical characteristics of field-effect transistors (FETs) based on polymer-sorted, large-diameter semiconducting carbon nanotube networks is investigated. The temperature dependences of both the carrier mobility and the source-drain current in the range of 78 K to 293 K indicate thermally activated, but non-Arrhenius, charge transport. The hysteresis in the transfer characteristics of FETs shows a simultaneous reduction with decreasing temperature. The hysteresis appears to stem from screening of charges that are transferred from the carbon nanotubes to traps at the surface of the gate dielectric. The temperature dependence of sheet resistance of the carbon nanotube networks, extracted from FET characteristics at constant carrier concentration, specifies fluctuation-induced tunneling as the mechanism responsible for charge transport, with an activation energy that is dependent on film thickness. Our study indicates inter-tube tunneling to be the bottleneck and implicates the role of the polymer coating in influencing charge transport in polymer-sorted carbon nanotube networks.

1. Introduction

Single-walled carbon nanotubes (SWCNTs) are promising materials for electronic device applications and have garnered tremendous interest in the last decade.[1–3] Even though the mobility of individual pristine semiconducting SWCNTs have been reported to be 100,000 $cm^2/V\,s$,[4] batches of as-synthesized carbon nanotubes, which always comprise a mixture of semiconducting and metallic species, have shown far inferior electrical properties. The presence of metallic tubes within carbon nanotube networks hampers the switching of field-effect transistors (FETs), and when present in quantities exceeding percolation thresholds, can even short-circuit the devices. Recently, progress in the preparation of semiconducting carbon nanotube "inks", namely dispersions of high purity semiconducting carbon nanotubes (s-SWCNTs), has in part brought us closer to realizing solution processable SWCNT network-based transistors with high on/off ratios.[5,6] Many macromolecule-based dispersants, such as single-stranded DNA,[7] DNA-based block co-polymers,[8] polythiophenes,[9] polyfluorene and its derivatives,[10–15] etc., have shown selectivity towards semiconducting carbon nanotubes. Compared to the commercially available counterpart of s-SWCNT dispersions that are prepared via density gradient ultracentrifuge, polymer-sorted s-SWCNTs dispersions are easier, less costly and less time-consuming to prepare. Recent studies have shown broad application of polymer-sorted s-SWCNTs in electronic devices, including FETs,[16–20] light-emitting transistors,[21] photodetectors and photovoltaics.[22–24] Recent work by Qian and co-workers has further demonstrated that FETs based on polymer-sorted s-SWCNTs can show comparable carrier mobility to those fabricated using commercially available semiconducting carbon nanotube inks.[19,25,26] Additional related work detailing polymer-wrapped SWCNTs and their applications in electronic devices are captured in a recent review.[27] So far, most studies have focused on understanding the structure of polymers and their selectivity for particular SWCNTs;[9–15] the preparation of SWCNT dispersions;[18–21] and the optimization of fabrication processes with the aim of improving the performance of devices comprising pre-sorted SWCNTs.[19,28] Issues, such as the nature of charge transport in such networks, remain largely unexplored.

In this present study, we examine the electrical characteristics of polymer-sorted s-SWCNTs-based transistors as a function of temperature and elucidate the carrier transport mechanism. We observe a decrease in carrier mobility of s-SWCNT network-based FETs and a simultaneous reduction in hysteresis with decreasing temperature. We also observe a correlation between the extent of hysteresis and the number of charges in the conduction channel, which suggests that the observed hysteresis originates from the screening of charges that are transferred from the carbon nanotubes to hydroxyl groups at the dielectric surface.[29] Temperature-dependent-resistance extracted from the I-V characteristics of FETs comprising polymer-sorted s-SWCNTs networks further suggest fluctuation-induced tunneling (FIT) as the mechanism responsible for charge transport.

2. Results and Discussion

Figure 1a shows the absorbance spectra of polymer-sorted s-SWCNTs and surfactant-dispersed carbon nanotubes normalized at the second optical transition of semiconducting carbon nanotubes at 1013 nm, and of pristine poly[(9,9-dioctylfluorenyl-2,7-diyl)-alt-co-(6,6′-{2,2′-bipyridine})], PFO-BPy, in toluene.

Dr. J. Gao, Prof. Y.-L. Loo
Department of Chemical and Biological Engineering
Princeton University Princeton
New Jersey 08544, United States
E-mail: lloo@princeton.edu

DOI: 10.1002/adfm.201402407

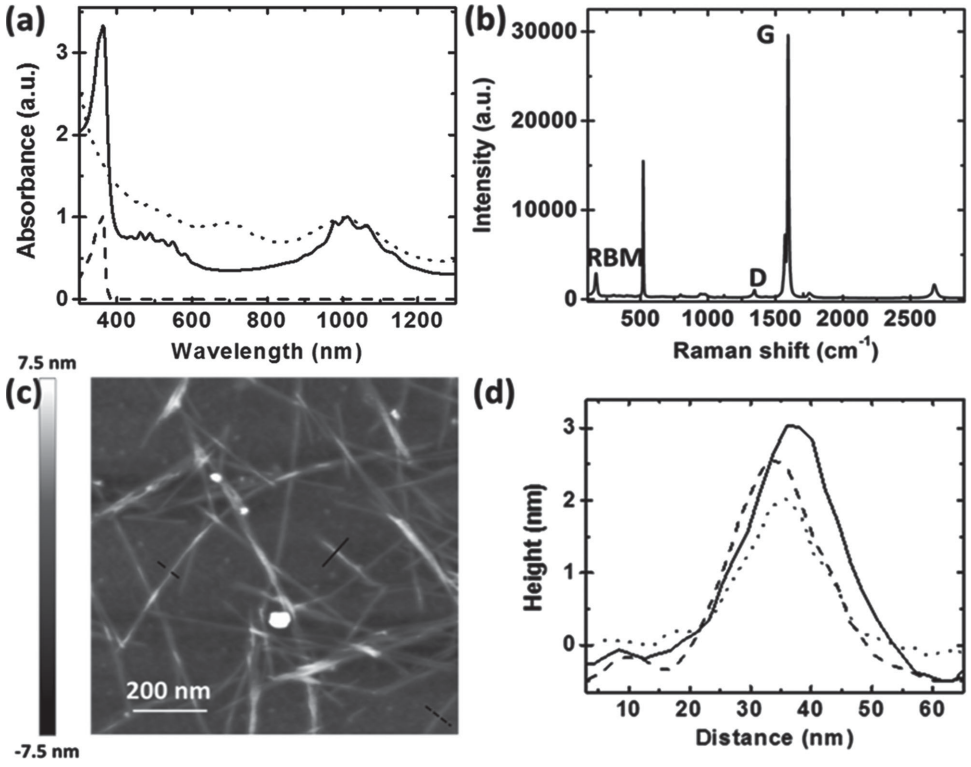

Figure 1. a) Optical absorption spectrum of polymer-sorted semiconducting carbon nanotubes (solid line) and surfactant-dispersed carbon nanotubes (dotted line) studied in this work normalized at the second optical transition of semiconducting carbon nanotubes at 1013 nm, and the pristine polymer (dashed line), normalized at the absorption peak at 363 nm. b) Raman spectrum of SWCNT films on Si/SiO_2 substrate. c) Atomic force microscopy (AFM) image of s-SWCNTs dispersed on a SiO_2 substrate. d) Height profile of three different SWCNTs from the AFM image showing the average diameter of polymer-sorted carbon nanotubes in the range of 2–3 nm.

The spectrum of sorted carbon nanotubes shows low absorbance in the 620–820 nm range. Since absorption in this region corresponds to the optical transition of metallic tubes, this observation evidences that PFO-BPy preferentially selects for semiconducting SWCNTs. Absorbance below 400 nm mainly originates from residual polymer; the absorption peak at 363 nm is the same as that in the spectrum of pristine polymer in toluene. In order to evaluate the weight ratio between PFO-BPy and the carbon nanotubes, we first calculated the absorption coefficient of PFO-BPy at its peak absorption in toluene (100.8 ml/mg-cm). The absorbance coefficient of semiconducting carbon nanotubes at its second optical transition peak at 1013 nm was estimated to be 36.5 ml/mg-cm, comparable to an absorbance coefficient of 34.9 ml/mg-cm that was reported at 937 nm.[30] Given the absorbance coefficients of the polymer and the dispersed carbon nanotubes, we back-estimated the weight ratio of PFO-BPy to carbon nanotubes in our dispersion to be 1.2. Figure 1b shows the Raman spectrum of a SWCNT film acquired with an excitation wavelength of 532 nm. This excitation wavelength is in resonance with semiconducting carbon nanotubes. The G band at 1590 cm^{-1} is attributed to tangential mode vibrations of the carbon atoms in the SWCNTs while the D band at 1340 cm^{-1} is attributed to the presence of defects and other disorder in the SWCNTs.[31] From the radial breathing mode (RBM) resonance at 168 cm^{-1} in the Raman spectrum, we estimated the diameter of the dispersed carbon nanotubes to be 1.4 nm.[32] Figure 1c shows an AFM image of sparse polymer-sorted SWCNTs deposited on SiO_2. Of 50 individual carbon nanotubes, we measured the average length to be 560 ± 140 nm. The average height was found to be in the range of 2–3 nm as shown in Figure 1d. That the average diameter of the polymer-sorted SWCNTs is larger than that estimated from the RBM mode in the Raman spectrum can be attributed to the presence of PFO-BPy that is presumed to wrap around the carbon nanotubes.

Figure 2a contains the transfer characteristics of a field-effect transistor having a 32-nm thick SWCNTs network in its channel (5 μm channel length) at different temperatures. The transistor shows p-type behavior as the gate bias is swept from 60 to −30 V. We observe a monotonic decrease in source-drain current (I_{DS}) with decreasing temperature, and a concomitant decrease in its threshold voltage from 33.4 V to 5.8 V. Figure 2b summarizes the source-drain currents at the on and off states of the transistor as a function of temperature. The on-state current, taken at gate bias (V_G) = −30 V, decreases from 23.7 μA at 293 K to 4.9 μA at 78 K; while the off-state current, taken at V_G = 60 V, also decreases, albeit more substantially by more than two orders of magnitude from 93.5 nA to 0.4 nA over the same temperature range. As a consequence, the on/off current ratio increases significantly from 250 at 293 K to 12250 at 78 K. That both the on- and off-state currents decrease with temperature indicates thermally activated charge transport and rules out the possibility that residual metallic SWCNTs are dictating transport in our devices.

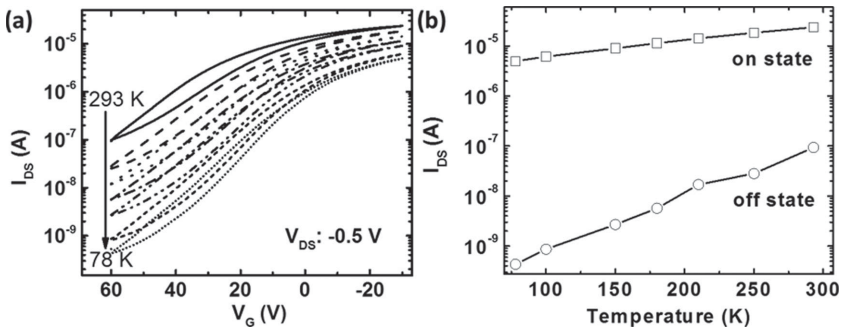

Figure 2. a) Representative transfer characteristics I_{DS}-V_G of device at V_{DS} = –0.5 V (W: 80 μm and L: 5 μm) in the temperature range of 78 K to 293 K. b) On- and off-state currents in polymer/s-SWCNT network-based FETs as a function of temperature.

Figure 3a summarizes the hole mobility and hysteresis in voltage in the aforementioned FET as a function of temperature. The hole mobilities were calculated from the transfer curve in the linear regime using Equation (1) below:

$$u = g_m \times \frac{L}{W} \times \frac{1}{C_{ox}} \times \frac{1}{V_{DS}} \quad (1)$$

where g_m is the transconductance, L and W are the channel length and width, respectively, of the transistor. V_{DS} is source-drain bias, and C_{ox} is the gate capacitance. Here we estimated the capacitance by assuming a dielectric constant of 11.5 nF/cm^2 for the 300-nm thick SiO_2 gate dielectric. With decreasing temperature, we observe a monotonic decrease in hole mobility from 4.3 cm^2/V s at 293 K to 1.4 cm^2/V s at 78 K. Interestingly, the decrease in mobility observed here cannot be adequately described by the Arrhenius temperature dependence over the entire temperature range (Arrhenius fit to the data shown in Figure S1 of Supporting Information). Specifically, the temperature dependence of mobility deviates substantially from the Arrhenius form at temperatures below 150 K, an observation we will elaborate upon later in this paper.

Additionally, we observe a simultaneous reduction in hysteresis upon cooling. For ease of comparison, we have defined hysteresis (ΔV) as the difference between the gate voltages needed to induce an average of the maximum and minimum drain currents during forward and reverse sweeps;[33] ΔV decreases from 6.1 V at 293 K to 1.5 V at 78 K. Previous studies have suggested that such hysteresis in SWCNTs-based FETs arises from defects at the carbon nanotube-dielectric interface.[34–36] Specifically, SWCNTs can act as leaky capacitors so carriers in the nanotubes can charge and discharge the hydroxyl groups on the dielectric surface. In the case of a p-type SWCNT FET, these hydroxyl groups trap electrons during the forward sweep and the trapped electrons increase screening of the gate dielectric, which in turn facilitates hole conduction. During the reverse sweep, the trapped electrons are released and they can combine with holes in the carbon nanotubes in the conduction channel. This action in turn causes a negative shift in threshold voltage. Vijayaraghavan and co-workers have accounted for such hysteresis with a capacitive charging model, in which the magnitude of the hysteresis is proportional to the number of carriers that are present in the device channel.[37] Inspired by this model, we explored the relationship between carrier concentration and device hysteresis in our carbon nanotube network-based FETs. Because the carrier concentration in a given FET channel is proportional to the ratio of conductance (G) and carrier mobility (u), or G/u, plotting the quantity G/(uΔV) should reveal the proportionality between carrier concentration and device hysteresis.[37] Figure 3b plots G/(uΔV) where u is extracted at V_G = 0 V as a function of temperature. That the average value is 1.3 ± 0.3 and invariant indicates that the proportionality between carrier concentration and device hysteresis is maintained over the entire temperature range. This analysis suggests that devices comprising polymer-sorted s-SWCNT also undergo the same trapping and detrapping mechanism under operation as that observed in other SWCNT FETs.

In order to verify that the temperature dependence of the electrical characteristics of s-SWCNT FETs is independent of channel length, we conducted similar measurements on devices having channel lengths that varied from 1 to 30 μm. In each case, we observed a decrease in the source-drain current, a negative shift in the threshold voltage and a reduction in hysteresis with decreasing temperature. We have also prepared and characterized FETs based on 7-nm thick SWCNT networks; these devices, too, showed the same temperature dependence with devices having 32-nm thick SWCNT networks. These experiments suggest the temperature dependence of electrical characteristics outlined above to be general and independent of device geometry.

Given that both the carrier concentration and the mobility contribute to the resistance extracted from the I-V characteristics of FETs, and the carrier concentration decreases with decreasing temperature in our devices, as evidenced by the negative threshold voltage (V_{th}) shift with decreasing temperature, we have chosen to examine the resistance at a constant carrier concentration to isolate the temperature dependence of mobility from that of

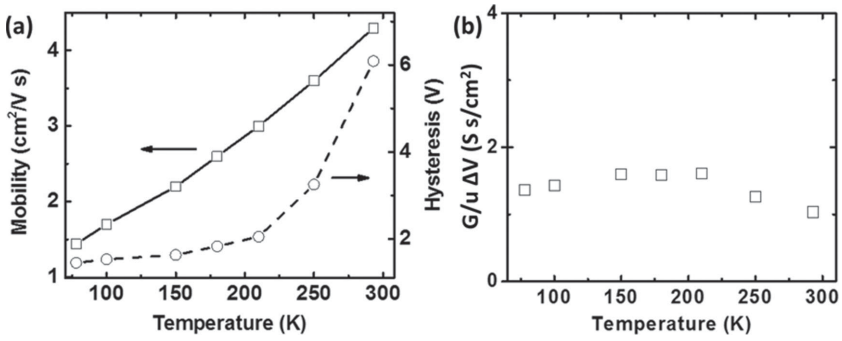

Figure 3. a) Hole mobility and hysteresis in polymer-sorted s-SWCNT network-based FET as a function of temperature; b) variation of the ratio of conductance (G) of s-SWCNT network, carrier mobility (u) at V_G = 0 V, and hysteresis (ΔV) in FETs with temperature.

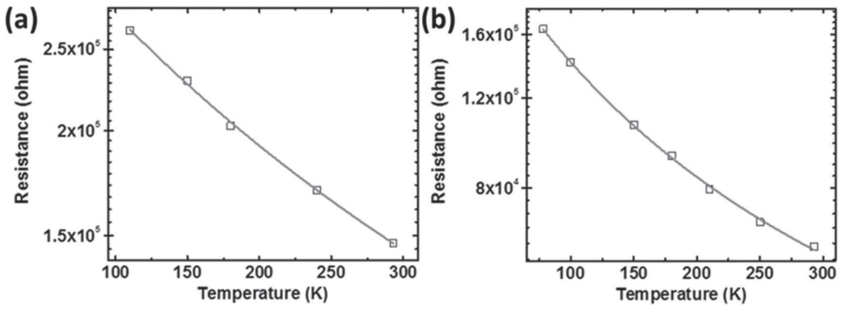

Figure 4. a) Temperature-dependent sheet resistance of a 7-nm thick s-SWCNT film; b) a 32-nm thick s-SWCNT film, extracted from I-V characteristics of FETs at V_G-V_{th} = −20 V. Symbols are experimental data and the solid lines are fits to the data using the fluctuation-induced tunneling (FIT) model.

the carrier concentration. We show in **Figure 4** the temperature dependence of resistance, extracted from the I-V characteristics of FETs having two different carbon nanotube network thicknesses at a constant carrier concentration, that is, at (V_G-V_{th}) of −20 V. Previous studies have shown charge transport in pristine carbon nanotube networks comprising both metallic and semiconducting carbon nanotubes to obey the variable-range hopping (VRH) model.[38] A recent report by Yanagi and co-workers demonstrated that transport in high purity SWCNT networks to also obey the VRH model, although the dimensionality of carrier hopping depends on the fraction of metallic carbon nanotubes in the networks. Indeed, charge transport in films that contain as little as 1% metallic SWCNTs can also be adequately described by the VRH model.[39] We thus initially expected charge transport in our polymer-wrapped semiconducting carbon nanotube networks to exhibit the same temperature dependence. We find instead the temperature dependence of our devices to be better described by the fluctuation induced tunneling (FIT) model of Sheng (VRH fits to our data are presented in Figures S2 and S3 of Supporting Information):[40]

$$R \propto \exp\left(\frac{T_1}{T+T_0}\right) \tag{2}$$

where R is the sheet resistance, T is temperature, T_1 is the temperature required for an electron to traverse the insulating gap and is thus proportional to the activation energy, and T_0 is the temperature above which thermally activated conduction over the barrier begins to occur. This model assumes a spatially parabolic energy barrier represented by $T_1 = 2SV_0 / \pi k_E e^2 w$, and $T_0 = 4\hbar SV_0^{3/2} / \pi^2 w^2 k_B e^2 \sqrt{2m}$, where S and w are the junction surface and width, respectively. V_0 is the depth of the potential well, m is the electron mass, e is the electron charge, k_B is Boltzmann constant and $h\left(\hbar = \frac{h}{2\pi}\right)$ is Planck constant. The temperature dependence of the FET mobility reported in Figure 3a also obeys the FIT model (data and fit shown in Figure S4 of Supporting Information).

This FIT model reduces to the Arrhenius temperature dependence when the temperature is above T_0. At temperatures below T_0, carriers cannot overcome the barrier so temperature-independent tunneling instead dominates. This model has been applied to a variety of systems with heterogeneous microstructures, including microcrystalline silicon,[41] TiO_2 thin films,[42] carbon nanotube bundles,[43] and carbon nanotube-polymer composites.[44] The study by Emmanuel and co-workers, for example, nicely demonstrates that transport in composite films comprising a mixture of metallic and semiconducting carbon nanotubes embedded in an insulating polymer matrix obeys the FIT model, when in the absence of the polymer matrix, transport is described by the VRH model. This finding thus implicates the role of the insulating polymer matrix in creating a transport barrier between individual carbon nanotubes.[44]

That charge transport in our polymer-sorted s-SWCNT networks obeys the FIT model as well suggests that the PFO-BPY coating similarly isolates individual carbon nanotubes. Different from macroscopic composites in which carbon nanotubes are dispersed in a polymer matrix, our carbon nanotube networks must be dispersed on a finer, molecular scale given our preparation technique. Compositionally, at a few weight percent loading, the macroscopic composites also comprise substantially less carbon nanotubes compared to our polymer-sorted semiconducting carbon nanotube networks (carbon nanotube loading estimated at 45 wt% based on absorbance). Yet, the similarity in temperature dependence of the resistance implicates inter-tube tunneling as the bottleneck to charge transport in both polymer-sorted semiconducting carbon nanotubes and in macroscopic carbon nanotube-polymer composites. Additional evidence supporting this claim stems from measurements on PFO-BPY-only FETs, which reveal the polymer to be electrically inactive. The presence of PFO-BPY on the surface of carbon nanotubes must thus isolate neighboring carbon nanotubes, effectively hindering inter-tube charge transport.

The best-fit parameters of T_1 and T_0 appear to be dependent on the thickness of polymer-sorted s-SWCNT film. We first observe a decrease in resistance with the increase in film thickness, which can be ascribed to an increased amount of conducting path. The parameters T_1 and T_0 were found to be 2457 K and 681 K in 7-nm thick SWCNT film and 1361 K and 318 K in 32-nm thick film, respectively. The decrease in T_1 translates to a decrease in activation energy from 0.21 eV to 0.12 eV with increasing film thickness. Considering the percolative nature of carbon nanotube networks, this activation energy must describe the overall barrier of the percolative path for charge transport between macroscopic electrodes. Compared to a thin s-SWCNT network, a thicker s-SWCNT network comprises more pathways for charge transport. The reduced activation energy measured in these films thus reflects the sampling of lower barrier pathways (i.e., pathways with less inter-tube junctions between electrodes) for macroscopic charge transport.

3. Conclusion

Our findings implicate the polymer dispersant to play a non-negligible role in charge transport of potentially commercially relevant polymer-sorted s-SWCNTs networks. The incorporation

of polymer dispersants having different electronic properties should thus impact charge transport of polymer sorted s-SWCNT networks accordingly.

4. Experimental Section

Dispersion: Polymer-sorted SWCNT dispersions were prepared following the procedure reported by Mistry et al.[30] Arc-discharge carbon nanotubes and poly[(9,9-dioctylfluorenyl-2,7-diyl)-alt-co-(6,6′-{2,2′-bipyridine})]), PFO-BPy, were obtained from Nanolab and American Dye Source, respectively. A solution, comprising 10 mL of toluene with 45 mg of raw SWCNTs and 45 mg of polymer, was sonicated for 30 min. We adopted a two-step ultracentrifuge process per Bisri et al., to extract the polymer-wrapped semiconducting-enriched carbon nanotubes, and then to further remove excess polymer from the sorted tubes.[18]

Device Fabrication: Bottom-gate, top-contact field-effect transistors comprising polymer-sorted SWCNT networks were fabricated on heavily doped Si substrate with a thermally grown 300-nm thick silicon dioxide as gate dielectric. Contact pads having Ti (5 nm)/Au (50 nm) were defined by standard photolithography, electron-beam evaporation and lift-off. We prepared SWCNT-based FETs by vacuum filtration. In this case, the SWCNT dispersion was filtered through 1.33 cm^2 mixed cellulose ester membranes (Millipore, pore size 220 nm). The filter cake comprising SWCNTs was then transferred onto Si/SiO_2 substrates with pre-defined contact pads by dissolving the membrane in acetone and methanol. E-beam lithography was performed to define palladium source/drain electrodes (70-nm thick) and to make electrical connections to the contact pads. A final photolithography step was performed to pattern the active channel region. Oxygen plasma treatment removed the SWCNTs outside the channel regions and electrically isolated neighboring devices.

Instruments: Absorbance measurements were performed on a Varian Cary 5000 spectrometer. Raman spectroscopy was performed using a Horiba ARAMIS Raman spectrometer with an excitation wavelength of 532 nm. Atomic Force Microscopic (AFM) images were collected using a Veeco Dimension NanoMan AFM. The average thicknesses of the carbon nanotube networks were measured using a KLA surface profilometer.

Electrical Characterization: SWCNT transistors were placed in a Lakeshore probe station (Lake Shore Cryotronics, Inc., Westerville, USA) and cooled with liquid nitrogen. The electrical characteristics were measured in vacuum ($< 5 \times 10^{-5}$ Torr) using an Agilent 4155C semiconductor parameter analyzer as a function of temperature from 293 K to 78 K. The device channel width was kept constant at 80 μm with variable channel lengths ranging from 1 to 30 μm.

Supporting Information

Supporting Information is available from the Wiley Online Library or from the author.

Acknowledgements

JG acknowledges the Netherlands Organisation for Scientific Research (NWO) for a Rubicon Post-doctoral Fellowship (Research Grant 680–50–1202). The authors acknowledge funding from NSF's Division of Chemistry (CHE-1124754) and from NRI (Gift # 2011-NE-2205GB) under the Nanoelectronics Beyond 2020 Initiative. The authors also thank Prof. R. K. Prud'homme and Prof. T. E. Shenk at Princeton University for access to their centrifuge facilities.

Received: July 18, 2014
Revised: September 22, 2014
Published online: October 14, 2014

[1] M. M. Shulaker, G. Hills, N. Pail, H. Wei, H.-Y. Chen, H.-S. P. Wong, S. Mitra, *Nature* **2013**, *501*, 526.
[2] Q. Cao, S.-J. Han, G. S. Tulevski, Y. Zhu, D. D. Lu, W. Haensch, *Nat. Nanotechnol.* **2013**, *8*, 180.
[3] S. J. Kang, C. Kocabas, T. Ozel, M. Shim, N. Pimparkar, M. A. Alam, S. V. Rotkin, J. A. Rogers, *Nat. Nanotechnol.* **2007**, *2*, 230.
[4] T. Duerkop, S. A. Getty, E. Cobas, M. S. Fuhrer, *Nano Lett.* **2004**, *4*, 35.
[5] M. C. Hersam, *Nat. Nanotechnol.* **2008**, *3*, 387.
[6] N. Rouhi, D. Jain, P. J. Burke, *ACS Nano* **2011**, *5*, 8471.
[7] X. Tu, S. Manohar, A. Jagota, M. Zheng, *Nature* **2009**, *460*, 250.
[8] M. Kwak, J. Gao, D. K. Prusty, A. J. Musser, V. A. Markov, N. Tombros, M. C. A. Stuart, W. R. Browne, E. J. Boekema, G. ten Brinke, H. T. Jonkman, B. J. van Wees, M. A. Loi, A. Herrmann, *Angew. Chem. Int. Ed.* **2011**, *50*, 3206.
[9] H. Lee, Y. Yoon, S. Park, J. H. Oh, S. Hong, L. S. Liyanage, H. Wang, S. Morishita, N. Patil, Y. J. Park, J. J. Park, A. Spakowitz, G. Galli, F. Gygi, P. H.-S. Wong, J. B.-H. Tok, J. M. Kim, Z. Bao, *Nat. Commun.* **2011**, *2*, 541.
[10] A. Nish, J. Y. Hwang, J. Doig, R. J. Nicholas, *Nat. Nanotechnol.* **2007**, *2*, 640.
[11] J. Gao, M. A. Loi, E. J. F. de Carvalho, M. C. Dos Santos, *ACS Nano* **2011**, *5*, 3993.
[12] J. Gao, M. Kwak, J. Wildeman, A. Herrmann, M. A. Loi, *Carbon* **2011**, *49*, 333.
[13] N. Berton, F. Lemasson, J. Tittmann, N. Stürzl, F. Hennrich, M. M. Kappes, M. Mayor, *Chem. Mater.* **2011**, *23*, 2237.
[14] H. Ozawa, T. Fujigaya, Y. Niidome, N. Hotta, M. Fujiki, N. Nakashima, *J. Am. Chem. Soc.* **2011**, *133*, 2651.
[15] J. Y. Hwang, A. Nish, J. Doig, S. Douven, C. W. Chen, L. C. Chen, R. J. Nicholas, *J. Am. Chem. Soc.* **2008**, *130*, 3543.
[16] N. Izard, S. Kazaoui, K. Hata, T. Okazaki, T. Saito, S. Iijima, N. Minami, *Appl. Phys. Lett.* **2008**, *92*, 243112.
[17] Z. Y. Liu, Z. J. Qiu, S. L. Zhang, Z. B. Zhang, *Adv. Mater.* **2012**, *24*, 3633.
[18] S. Z. Bisri, J. Gao, V. Derenskyi, W. Gomulya, I. Iezhokin, P. Gordiichuk, A. Herrmann, M. A. Loi, *Adv. Mater.* **2012**, *24*, 6147.
[19] L. Qian, W. Xu, X. Fan, C. Wang, J. Zhang, J. Zhao, Z. Cui, *J. Phys. Chem. C* **2013**, *117*, 18243.
[20] W. Gomulya, G. D. Costanzo, E. J. F. de Carvalho, S. Z. Bisri, V. Derenskyi, M. Fritsch, N. Fröhlich, S. Allard, P. Gordiichuk, A. Herrmann, S. J. Marrink, M. C. dos Santos, U. Scherf, M. A. Loi, *Adv. Mater.* **2013**, *25*, 2948.
[21] F. Jakubka, C. Backes, F. Gannott, U. Mundloch, F. Hauke, A. Hirsch, J. Zaumseil, *ACS Nano* **2013**, *7*, 7428.
[22] M. S. Arnold, J. D. Zimmerman, C. K. Renshaw, X. Xu, R. R. Lunt, C. M. Austin, S. R. Forrest, *Nano Lett.* **2009**, *9*, 3354.
[23] D. J. Bindl, N. S. Safron, M. S. Arnold, *ACS Nano* **2010**, *4*, 5657.
[24] S. Ren, M. Bernardi, R. R. Lunt, V. Bulovic, J. C. Grossman, S. Gradecak, *Nano Lett.* **2011**, *11*, 5316.
[25] M. Engel, J. P. Small, M. Steiner, M. Freitag, A. A. Green, M. C. Hersam, Ph. Avouris, *ACS Nano* **2008**, *2*, 2445.
[26] M. Ha, Y. Xia, A. A. Green, W. Zhang, M. J. Renn, C. H. Kim, M. C. Hersam, C. D. Frisbie, *ACS Nano* **2010**, *4*, 4388.
[27] W. Gomulya, J. Gao, M. A. Loi, *Eur. Phys. J. B* **2013**, *86*, 404.
[28] V. K. Sangwan, R. P. Ortiz, J. M. P. Alaboson, J. D. Emery, M. J. Bedzyk, L. J. Lauhon, T. J. Marks, M. C. Hersam, *ACS Nano* **2012**, *6*, 7480.
[29] J. S. Lee, S. Ryu, K. Yoo, I. S. Choi, W. S. Yun, J. Kim, *J. Phys. Chem. C* **2007**, *111*, 12504.
[30] K. S. Mistry, B. A. Larsen, J. L. Blackburn, *ACS Nano* **2013**, *7*, 2231.
[31] M. S. Dresselhaus, G. Dresselhaus, R. Saito, A. Jorio, *Phys. Rep.* **2005**, *409*, 47.
[32] J. C. Meyer, M. Paillet, T. Michel, A. Moreac, A. Neumann, G. S. Duesberg, S. Roth, J. L. Sauvajol, *Phys. Rev. Lett.* **2005**, *95*, 217401.

[33] S. H. Jin, A. E. Islam, T. I. Kim, J. H. Kim, M. A. Alam, J. A. Rogers, *Adv. Funct. Mater.* **2012**, *22*, 2276.
[34] S. A. McGill, S. G. Rao, P. Manandhar, P. Xiong, S. Hong, *Appl. Phys. Lett.* **2006**, *89*, 163123.
[35] H. G. Ong, J. W. Cheah, X. Zou, B. Li, X. H. Cao, H. Tantang, L.-J. Li, H. Zhang, G. C. Han, J. Wang, *J. Phys. D: Appl. Phys.* **2011**, *44*, 285301.
[36] S. Kar, A. Vijayaraghavan, C. Soldano, S. Talapatra, R. Vajtai, O. Nalamasu, P. M. Ajayan, *App. Phys. Lett.* **2006**, *89*, 132118.
[37] A. Vijayaraghavan, S. Kar, C. Soldano, S. Talapatra, O. Nalamasu, P. M. Ajayan, *App. Phys. Lett.* **2006**, *89*, 162108.
[38] A. B. Kaiser, V. Skakalova, *Chem. Soc. Rev.* **2011**, *40*, 3786.
[39] K. Yanagi, H. Kataura, H. Udoguchi, T. Ishida, S. Sagitani, K. Matsuda, Y. Oshima, T. Takenobu, Y. Maniwa, *ACS Nano* **2010**, *4*, 4027.
[40] P. Sheng, *Phys. Rev. B* **1980**, *21*, 2180.
[41] S. J. Konezny, M. N. Bussac, L. Zuppiroli, *Appl. Phys. Lett.* **2008**, *92*, 012107.
[42] S. J. Konezny, C. Richter, R. C. Snoeberger, A. R. Parent, G. W. Brudvig, C. A. Schmuttenmaer, V. S Batista, *J. Phys. Chem. Lett.* **2011**, *2*, 1931.
[43] M. Salvato, M. Cirillo, M. Lucci, S. Orlanducci, I. Ottaviani, M. L. Terranova, F. Toschi, *Phys. Rev. Lett.* **2008**, *101*, 246804.
[44] K. Emmanuel, A. J. A. Gehan, *J. Appl. Phys.* **2006**, *99*, 084302.